Evaluation of Magnetic Structure of Ultrathin Mn_4N Films by X-Ray Magnetic Circular Dichroism Analysis

Mn_4N epitaxial thin films with a thickness of 4.2 nm were prepared on $SrTiO_3$(001) substrates. A thickness-dependent sign reversal of the anomalous Hall effect was observed. X-ray magnetic circular dichroism measurements at room temperature suggest that the magnetic structure of Mn_4N with a thickness of about 4 nm contains a noncollinear magnetic component different from that of conventional ferrimagnetic Mn_4N films. Furthermore, the ultrathin Mn_4N film exhibits smaller magnetization than the 24.7 nm thick Mn_4N film with a conventional magnetic structure, as confirmed by magneto-optical sum rule analysis.

Anti-perovskite Mn_4N is a candidate for current-driven domain wall (DW) motion devices such as a nonvolatile memory and a logic circuit. It exhibits a perpendicular anisotropy of K_u ~ 0.1 MJ m^{-3}, a small spontaneous magnetization of M_s ~ 80 kA m^{-1} [1], and a high thermal stability with the Néel temperature of 740 °C [2]. Experiments with microstrips of Mn_4N-based materials demonstrated a high-speed DW motion driven by spin-transfer torques (STTs) at room temperature (RT) [1]. However, the current density for DW motion was large (j > 3×10^{11} A/m^{-2}). To suppress the driving current, we have explored the use of spin-orbit torques (SOTs), which allows for more efficient DW motion than STTs. To achieve SOT-driven DW motion of Mn_4N without an external field, it is necessary to fabricate Mn_4N ultrathin films. In this study, we focused on the fabrication of Mn_4N ultrathin films on $SrTiO_3$(001) substrates and the evaluation of magnetic properties at room temperature (RT).

The $SrTiO_3$ substrates were etched with buffered HF solution to obtain a flat surface. The Mn_4N films were fabricated using the plasma-assisted molecular beam epitaxy method, where Mn atoms and N plasma were supplied simultaneously. The thickness of the Mn_4N layer was controlled by the deposition time. They were determined as 24.7 nm for Sample A and 4.2 nm for Sample B by X-ray reflectometry (XRR) results shown in **Fig. 1(a)**. After the deposition of Mn_4N, the reflection high-energy electron diffraction (RHEED) images were taken along the $SrTiO_3$[100] azimuth. They showed sharp streak patterns originating from the high-quality epitaxial growth of the Mn_4N layer on $SrTiO_3$(001) for both samples. The Mn_4N layer was covered by a SiO_2 capping layer deposited by radio-frequency sputtering to prevent the oxidation of Mn_4N. The surfaces of both samples were smooth as confirmed by atomic force microscopy (AFM). **Figure 1(d)** shows the result of the anomalous Hall effect (AHE) measurement when a magnetic field to the surface was applied. The thickness-dependent sign reversal in the AHE indicates a difference in magnetic structure.

Figures 2 show the results of X-ray absorption spectroscopy (XAS) and X-ray magnetic circular dichroism (XMCD) measurements for Mn $L_{2,3}$ absorption edges at RT. The measurements were performed by the total electron yield (TEY) method. Circularly polarized X-rays and a magnetic field of 5 T were applied from θ ~ 55° (magic angle) relative to the surface

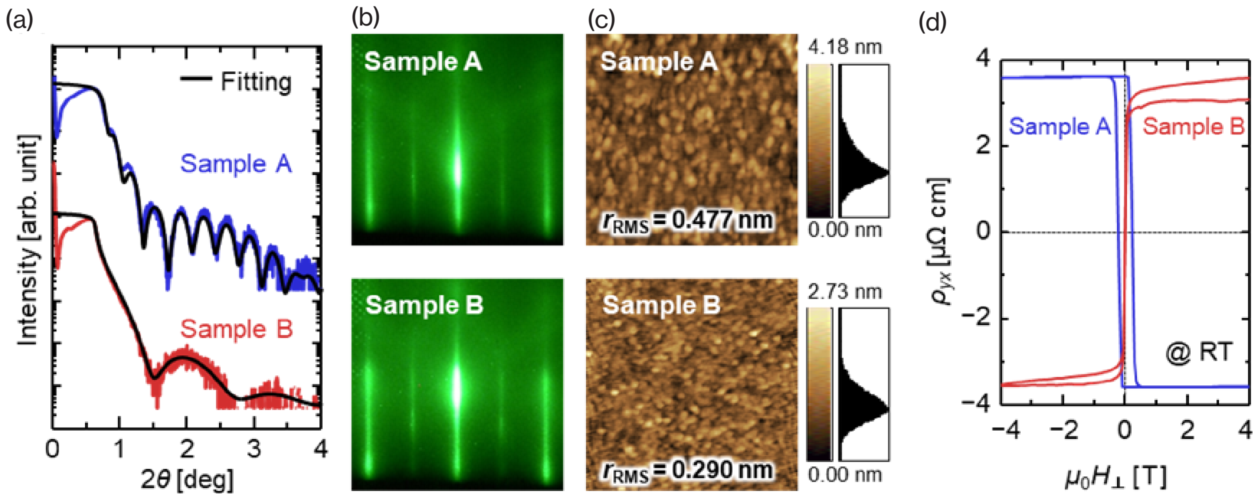

Figure 1: **(a)** XRR profiles and the fitting results. Blue and red lines indicate the measured profiles of Samples A and B, respectively. Black lines show fitting results. **(b)** RHEED images for Mn_4N layers along the $SrTiO_3$[100] azimuth. **(c)** AFM images with a scan range of 1 μm square. **(d)** Anomalous Hall resistivities ρ_{yx} at RT.

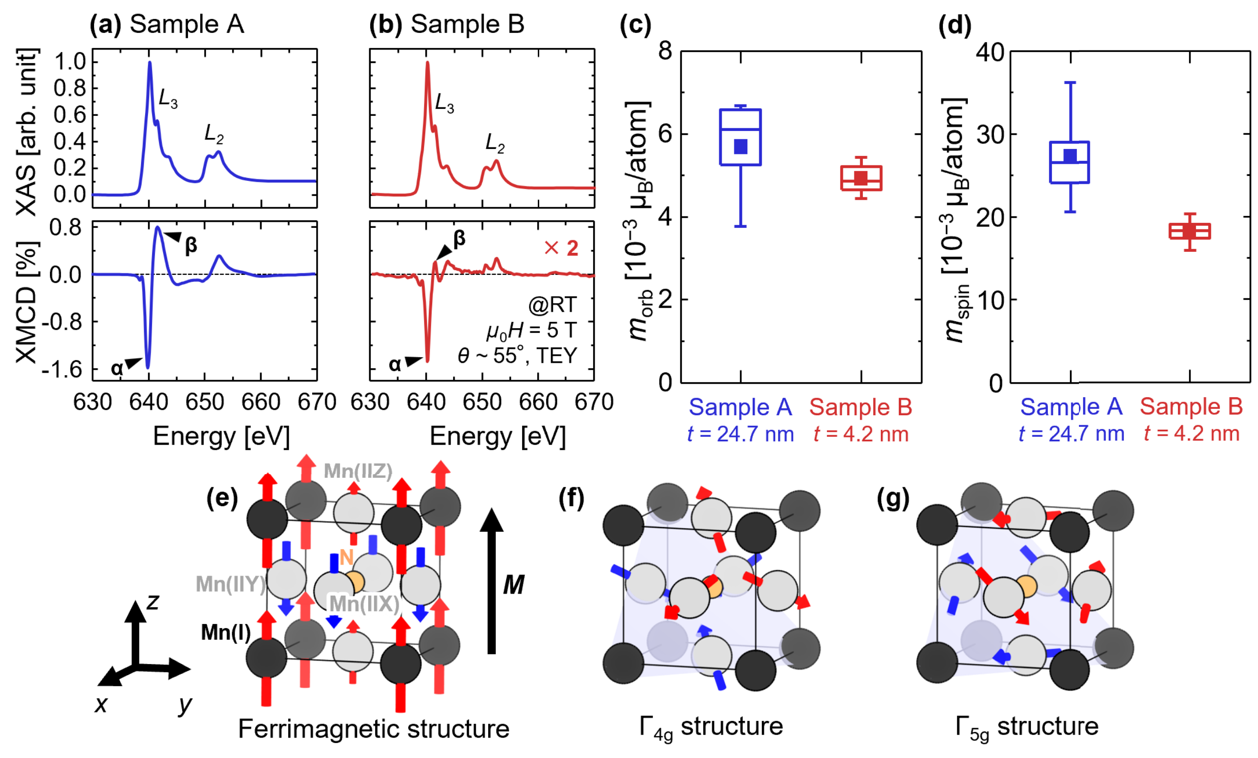

Figure 2: Results of XAS and XMCD measurements. **(a, b)** XAS and XMCD spectra of Samples A and B obtained at RT. **(c)** Orbital magnetic moments and **(d)** spin magnetic moments obtained using the magneto-optical sum rule. **(e)** Conventional ferrimagnetic structure of Mn_4N film. **(f, g)** Noncollinear magnetic structures of anti-perovskite crystal categorized as Γ_{4g} and Γ_{5g}.

normal. The XMCD spectrum of Sample A in **Fig. 2(a)** shows a profile attributed to the ferrimagnetism of Mn_4N (**Fig. 2(e)**). The negative sharp peak α in the Mn L_3 absorption edge is mainly derived from corner Mn(I) with a magnetic moment parallel to the magnetization. The positive broad peak β is mainly derived from face-centered Mn(IIX, IIY) with antiparallel magnetic moments [3]. On the other hand, the XMCD spectrum of Sample B in **Fig. 2(b)** showed a reduced overall intensity. In particular, the peak α was visible at the L_3 absorption edge, but the peak β was significantly attenuated. These results suggest that the magnetic structure depends on the thickness of the Mn_4N layer. The orbital (**Fig. 2(c)**) and spin (**Fig. 2(d)**) magnetic moments of Mn atoms were calculated using the magneto-optical sum rule [4]. Focusing on spin magnetic moment m_{spin} which dominated the magnetization, it is evident that the m_{spin} of Sample B is smaller than that of Sample A. This may have been caused by changes in the magnetic structure and the Néel temperature. According to the literature by D. Fruchart *et al.* [5], the magnetic structure of bulk Mn_4N contains noncollinear texture components such as Γ_{4g} in **Fig. 2(f)** and Γ_{5g} in **Fig. 2(g)**. For Mn_4N thin films, the noncollinear component is usually negligible, and a collinear ferrimagnetic structure (**Fig. 2(e)**) is often considered. However, in ultrathin Mn_4N films, the noncollinear component may become significant, canceling the magnetic moment of Mn(II) and reducing the intensity of peak β in XMCD (**Fig. 2(b)**).

In summary, we have demonstrated the epitaxial growth of high-quality ultrathin Mn_4N films on $SrTiO_3$(001) substrates. The thickness-dependent change of magnetic structures was confirmed by AHE and XMCD spectra. The XMCD spectra of 4.2-nm-thick Mn_4N film indicated the presence of a noncollinear magnetic component.

REFERENCES

[1] T. Gushi, M. Jovičević Klug, J. Peña Garcia, S. Ghosh, J. -P. Attané, H. Okuno, O. Fruchart, J. Vogel, T. Suemasu, S. Pizzini and L. Vila, *Nano Lett.* **19**, 8716 (2019).
[2] C. Li, Y. Yang, L. Lv, H. Huang, Z. Wang and S. Yang, *J. Alloys Compd.* **457**, 57 (2008).
[3] K. Ito, Y. Yasutomi, S. Zhu, M. Nurmamat, M. Tahara, K. Toko, R. Akiyama, Y. Takeda, Y. Saitoh, T. Oguchi, A. Kimura and T. Suemasu, *Phys. Rev. B* **101**, 104401 (2020).
[4] P. Carra, B. T. Thole, M. Altarelli and X. Wang, *Phys. Rev. Lett.* **70**, 694 (1993).
[5] D. Fruchart, D. Givord, P. Convert, P. L'héritier and J. P. Sénateur, *J. Magn. Magn. Mater.* **15-18**, 490 (1980).

BEAMLINE

BL-16A

T. Yasuda[1], K. Amemiya[2] and T. Suemasu[1] ([1]Univ. of Tsukuba, [2]KEK-IMSS)